

Onset and manipulation of self-assembled morphology in freely standing polymer trilayer films

Chris A. Murray, Stephen W. Kamp, Jason M. Thomas, and John R. Dutcher*

Department of Physics and the Guelph-Waterloo Physics Institute, University of Guelph, Guelph, Ontario, Canada N1G 2W1

(Received 19 August 2003; revised manuscript received 3 March 2004; published 23 June 2004; publisher error corrected 30 June 2004)

We have used reflected light microscopy to study the lateral morphology which self-assembles at elevated temperatures in films consisting of a polyisoprene (PI) layer capped on both sides by polystyrene (PS) layers: freely standing PS/PI/PS trilayer films. Heating of the trilayer films causes the formation of a periodic, lateral morphology which is driven by the attractive dispersion interaction acting across the film. In our studies of the temperature dependence of the morphology, we find that the onset temperature for the formation of the morphology increases with increasing heating rate. By heating the films to temperatures greater than the glass transition temperature of the PS-capping layers, the morphology is removed. By heating and then cooling the films, the morphology formed upon heating disappears and reforms at right angles to the original morphology with a larger periodicity characteristic of the lower temperature. These results can be explained by considering the time and temperature dependence of Young's modulus of PS.

DOI: 10.1103/PhysRevE.69.061612

PACS number(s): 68.15.+e, 68.55.Jk, 68.60.Dv

I. INTRODUCTION

Thin polymer films with thicknesses of tens of nanometers are studied extensively for two reasons: (1) they provide an ideal sample geometry for studying the effects of one-dimensional confinement on the structure, morphology, and dynamics of the polymer molecules, and (2) they are used extensively in technological applications such as optical coatings, protective coatings, adhesives, barrier layers, and packaging materials. The stability of the films is a key issue in all of these studies and applications. For most applications, it is necessary to ensure that the film remains stable within its range of operating temperatures. However, by exploiting instabilities that are inherent to thin polymer films in response to changes in, e.g., temperature and applied fields, it is possible to achieve unique applications such as multilayer active packaging materials and well-ordered, self-assembled morphologies in the plane of the film with micrometer- and even nanometer-length scales.

Thin polymer films can be susceptible to the formation of holes when heated to temperatures that are comparable to or greater than the bulk glass transition temperature T_g^B for which considerable chain mobility is obtained. In the absence of external fields, the instability can be driven by the van der Waals or dispersion interaction which can be substantial for film thicknesses $h < 100$ nm [1]. For films supported on substrates, it is possible for the dispersion interaction between the two film surfaces to be attractive, such that the uniform film breaks up into droplets via a process known as dewetting [2,3], or repulsive, which enhances the stability of the films [1]. Unsupported or freely standing polymer films are always unstable to the formation and growth of holes at elevated temperatures [4–6], since the dispersion interaction is always attractive for this film geometry which is symmetric about the midplane of the film [1]. Holes can

form via two different mechanisms: they can be nucleated by external perturbations or defects, such as dust or density inhomogeneities, or they can form spontaneously due to amplification of long-wavelength fluctuations of the film surfaces driven by the attractive dispersion interaction between the two film surfaces. In the case of nucleation, holes with radii R greater than a critical value R_c grow with time, where $R_c = h/2$ [7]. In the case of spontaneous hole formation, holes can form in the film due to the interplay between the dispersion interaction and the surface tension contributions to the free energy [8].

One way to improve the thermal stability of freely standing polymer films is to add solid capping layers to both film surfaces, creating a freely standing trilayer film [9]. Upon heating, it is found that a distinctive morphology forms spontaneously in the plane of the film, consisting of long, parallel domains with a well-defined periodicity. The domains are formed when the capping layers come together to pinch off tubes of the fluid central layer. This phenomenon occurs for a wide variety of material combinations, for both freely standing [9] and supported [9–11] films, with only two requirements: the capping layers must be solid, but thin enough to be deformable at a temperature for which the central layer is in the melt phase, and the dispersion force must be attractive and large enough to drive the morphology. As discussed below, an analysis of the initial stages of the instability leading to the in-plane morphology showed that the wavelength that grows most rapidly is given by $\lambda_m = \sqrt[4]{3}\lambda_c$ [9], where λ_c is the critical wavelength above which it is energetically favorable for the amplitude of the instability to grow with time. Also, the dependence of the wavelength of the lateral morphology λ_m on the individual film thicknesses (central layer thickness h , capping layer thickness L) was predicted to be $\lambda_m \propto L^{3/4}(h+2L)$, and this relationship was shown to be satisfied for $\text{SiO}_x/\text{PS}/\text{SiO}_x$ freely standing films with $30 \text{ nm} < h < 121 \text{ nm}$ and $17.7 \text{ nm} < L < 30.4 \text{ nm}$ [9].

Microscopic self-assembled pattern formation has also been observed in supported homopolymer films and block copolymer films that have been heated to temperatures above

*Author to whom correspondence should be addressed. Electronic address: dutcher@physics.uoguelph.ca

the bulk glass transition temperature and subjected to electric fields and thermal gradients [12,13]. In general, relatively thick films were used in these studies such that the dispersion interaction acting across the film was very small and the morphology was driven by the application of external fields. It has also been shown that tailored micron-scale patterning is possible without the application of an external electric field by placing the film in the gap between patterned templates [14,15].

Recently, we investigated self-assembly and pattern formation in freely standing polymer trilayer films consisting of a thin layer of polyisoprene (PI) capped on both sides by polystyrene (PS) layers, which we refer to as PS/PI/PS trilayer films. We have demonstrated that the lateral morphology forms at right angles to cracks in the PS layers, which can be exploited to produce square arrays of isolated micron-size droplets of PI separated by and encapsulated between the PS capping layers [16]. In the present study, we have measured the dependence on the heating rate of the temperature T_{onset} corresponding to the onset of morphology formation and we have explored the dependence of the stability of the morphology on the thermal history of the films. If the trilayer films are heated from room temperature to temperatures greater than the bulk glass transition temperature T_g^B for PS, the lateral morphology first appears at temperatures much less than T_g^B and then disappears at temperatures comparable to T_g^B . The lateral morphology can also be modified by cooling the films. If a film is heated quickly to a temperature less than T_g^B , lateral morphology will begin to form with a certain wavelength. If the film is then cooled to a lower temperature, the original morphology disappears and a new morphology with a larger wavelength forms at right angles to the original morphology. The dependence of T_{onset} on the heating rate and the changes in morphology obtained upon further heating or cooling of the trilayer films can be understood by considering the time and temperature dependence of Young's modulus of the PS capping layers.

II. INITIAL STAGES OF INSTABILITIES IN FREELY STANDING POLYMER FILMS

To understand the initial stages of instability of freely standing polymer trilayer films at different temperatures, we will make use of two calculations from the literature: spontaneous hole formation in freely standing single layer fluid films [8], for which the interactions that determine the nature of the instability are surface tension and dispersion, and spontaneous morphology formation in freely standing trilayer films with a fluid central layer capped symmetrically by layers of a solid material [9], for which the interactions that determine the nature of the instability are dispersion and the elastic bending of the solid capping layers. For both cases, we use a linear stability analysis to examine the initial stages of instabilities in the films.

A. Freely standing single-layer fluid films

For freely standing single-layer fluid films of thickness h_0 , we consider the stability of sinusoidal undulations $\zeta \cos qx$

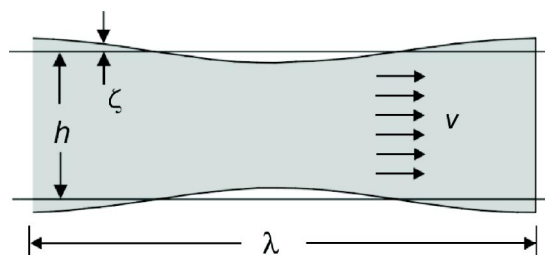


FIG. 1. A schematic view of a thin polymer single-layer film with a sinusoidal undulation in the air/polymer interfaces.

of the film surfaces that are symmetric about the midplane of the film (see Fig. 1), where $q=2\pi/\lambda$. The average change in the free energy $\langle \Delta E \rangle$ can be written as the sum of the average free energy change due to the creation of new area on the two surfaces (ΔE_{surf}) and the average free energy change due to the dispersion interaction (ΔE_{disp}):

$$\begin{aligned} \langle \Delta E \rangle &= \langle \Delta E_{surf} \rangle + \langle \Delta E_{disp} \rangle \\ &= \frac{2\gamma}{\lambda} \left\{ \int_0^\lambda \left[1 + \frac{1}{2} \left(\frac{dy}{dx} \right)^2 \right] dx - \lambda \right\} \\ &\quad - \frac{A}{12\pi\lambda} \left[\int_0^\lambda \left(\frac{1}{h^2} - \frac{1}{h_0^2} \right) dx \right], \end{aligned} \quad (1)$$

where γ is the surface tension, $y=\zeta \cos qx$ is the undulation in one of the film surfaces, the film thickness $h=h_0+2\zeta \cos qx$, h_0 is the unperturbed film thickness, A is the Hamaker coefficient which characterizes the dispersion interaction [1], and $\langle \dots \rangle$ refers to averaging over one wavelength λ of the undulation. In the limit of small-amplitude undulations ($\zeta \ll h_0$), Eq. (1) can be written as

$$\langle \Delta E \rangle = \left[\frac{q^2 \gamma}{2} - \frac{A}{2\pi h_0^4} \right] \zeta^2. \quad (2)$$

The average energy change given by Eq. (2) is equal to zero for a critical value of the wave vector $q=q_c$:

$$q_c = \frac{2\pi}{\lambda_c} = \sqrt{\frac{A}{\pi\gamma h_0^4}}. \quad (3)$$

For wavelengths $\lambda > \lambda_c$, it is energetically favorable for the undulation amplitude to grow; for $\lambda < \lambda_c$, it is energetically favorable for the undulation amplitude to decay to zero.

B. Freely standing trilayer films with solid capping layers

For freely standing trilayer films consisting of a fluid central layer of thickness h_0 which is capped symmetrically by solid capping layers of thickness L , we consider sinusoidal undulations $\zeta \cos qx$ of the film surfaces that are symmetric about the midplane of the film (see Fig. 2), where the wave vector $q=2\pi/\lambda$. The average change in the free energy $\langle \Delta E \rangle$ can be written as the sum of the average free energy change due to the bending of the solid capping layers (ΔE_{bend}) and the average free energy change due to the attractive dispersion interaction acting across the entire trilayer film thickness (ΔE_{disp}) [1,17]:

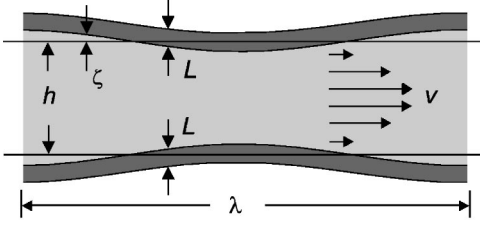


FIG. 2. A schematic view of a thin polymer trilayer film with a sinusoidal undulation in the air/polymer interfaces.

$$\begin{aligned} \langle \Delta E \rangle &= \langle \Delta E_{\text{bend}} \rangle + \langle \Delta E_{\text{disp}} \rangle \\ &= \frac{YL^3}{24\lambda(1-\sigma^2)} \left[\int_0^\lambda \left(\frac{d^2y}{dx^2} \right)^2 dx \right] \\ &\quad - \frac{A}{12\pi\lambda} \left[\int_0^\lambda \left(\frac{1}{(h+2L)^2} - \frac{1}{(h_0+2L)^2} \right) dx \right], \quad (4) \end{aligned}$$

where Y and σ are the Young's modulus and Poisson's ratio for the capping layer material, L is the capping layer thickness, h_0 is the unperturbed central layer thickness, $h = h_0 + 2\zeta \cos qx$ is the perturbed central layer thickness, and $\langle \dots \rangle$ refers to an average over one wavelength λ of the undulation. In the limit of small-amplitude undulations ($\zeta \ll h_0$), Eq. (4) can be written as

$$\langle \Delta E \rangle = \left[\frac{YL^3}{24(1-\sigma^2)} q^4 - \frac{A}{2\pi(h_0+2L)^4} \right] \zeta^2. \quad (5)$$

The average energy change given by Eq. (5) is equal to zero for a critical value of the wave vector q_c :

$$q_c = \frac{2\pi}{\lambda_c} = \sqrt[4]{\frac{12A(1-\sigma^2)}{\pi Y L^3 (h_0+2L)^4}}. \quad (6)$$

For wavelengths $\lambda > \lambda_c$, it is energetically favorable for the undulation amplitude to grow; for $\lambda < \lambda_c$, it is energetically favorable for the undulation amplitude to decay to zero.

The dynamics of the self-assembly process can be analyzed by considering the effect of pressure gradients in the central fluid layer in the presence of sinusoidal undulations [9]. The pressure in the central fluid layer has two contributions: the pressure P_D induced by the dispersion force acting across the entire trilayer film thickness which drives the morphology and the pressure P_B due to the bending of the capping layers. The pressure P on the fluid can be written as [1,17]

$$\begin{aligned} P = P_B + P_D &\approx \frac{A}{6\pi(h_0+2L)^3} \\ &+ \left[D(\nabla^2)^2 - \frac{A}{\pi(h_0+2L)^4} \right] \zeta \cos qx, \quad (7) \end{aligned}$$

where $D = (YL^3)/[12(1-\sigma^2)]$, Y and σ are the Young's modulus and Poisson's ratio of the capping layer material, and A is the Hamaker coefficient associated with the capping layer-air interfaces.

Pressure gradients within the fluid film produce flow of the fluid, squeezing the fluid out of the regions where the capping layer separation is decreased ($\zeta < 0$). We assume Poiseuille flow with no slippage at the fluid capping layer boundaries. This simple fluid analysis is a useful first-order approximation for a polymer melt at very high temperatures. The pressure gradient for the parabolic flow field is

$$\begin{aligned} -\vec{\nabla} P &= \frac{2}{h_0} \times (\text{edge stress}) \\ &= \frac{2}{h_0} \eta \left. \frac{\partial \vec{v}}{\partial z} \right|_{\text{edge}} \\ &= \frac{8\eta}{h_0^2} \vec{v}_m, \quad (8) \end{aligned}$$

where \vec{v} is the fluid velocity, \vec{v}_m is the maximum velocity obtained at the midplane of the fluid film, η is the viscosity, and the z direction is chosen normal to the film. Combining Eqs. (7) and (8) and the continuity equation which reduces to $\vec{\nabla} \cdot \vec{v}_m = -(3/h_0)(\partial \zeta / \partial t) \cos qx$, we obtain

$$\frac{24\eta}{h_0^3} \frac{\partial \zeta}{\partial t} \cos qx = \nabla^2 \left[D(\nabla^2)^2 - \frac{A}{\pi(h_0+2L)^4} \right] \zeta \cos qx. \quad (9)$$

We assume that the amplitude of the capping layer deformation depends exponentially on time, $\zeta \sim e^{t/\tau}$, with time constant τ . Substituting this assumed time dependence for ζ into Eq. (9), we obtain

$$\frac{1}{\tau} \frac{24\eta}{h_0^3} = -Dq^6 + \frac{Aq^2}{\pi(h_0+2L)^4}. \quad (10)$$

There is exponential growth of the deformation for wave vectors $q < q_c$, given by Eq. (6). The wave vector q_m that grows most rapidly can be obtained by differentiating Eq. (10) with respect to q and setting the result equal to zero. We find that $q_m = q_c / \sqrt[4]{3}$, with corresponding wavelength

$$\lambda_m = \frac{2\pi}{q_m} = 2\pi \sqrt[4]{\frac{\pi Y}{4A(1-\sigma^2)}} L^{3/4} (h_0+2L). \quad (11)$$

The characteristic growth time τ corresponding to the wavelength λ_m that grows most rapidly can be obtained by substituting the expression for q_m into Eq. (10):

$$\tau = 18\eta \left[\frac{\pi^3 Y}{A(1-\sigma^2)} \right]^{1/2} \frac{L^{3/2}}{h_0^3} (h_0+2L)^6. \quad (12)$$

III. EXPERIMENT

A. Sample preparation

Narrow-distribution polystyrene (molecular weight of $\bar{M}_w = 718 \times 10^3$ g/mol and polydispersity index $M_w/M_n = 1.12$) and *cis*-1,4-polyisoprene (molecular weight of $\bar{M}_w = 414 \times 10^3$ g/mol and $M_w/M_n = 1.06$) were obtained from Polymer Source Inc. The freely standing PS/PI/PS trilayer

films were prepared in a multistep process using a combination of spin-coating and water-transfer techniques. The water-transfer procedure [18] used distilled water produced by a Millipore system and was performed in a clean environment (laminar flow cabinet). Thin PS films were prepared on freshly cleaved Muscovite mica substrates by spincoating solutions of PS dissolved in toluene. Solutions with PS mass concentrations of 1.4%–1.7% were spin coated at speeds of 3000–4000 rpm to obtain the PS film thicknesses L used in this study: $60 \text{ nm} < L < 86 \text{ nm}$. After spin-coating, the PS films on the mica substrates were annealed in vacuum at 115°C for 12 h. The annealing procedure is performed to remove any solvent that may be trapped in the films as well as to allow the chains to relax after the spin-coating procedure. The samples were then cooled to room temperature at a rate of $1^\circ\text{C}/\text{min}$. For each PS film thickness, three or more films were prepared on mica. One PS film was transferred onto a distilled water surface and then captured on a Si wafer for subsequent measurement of the film thickness using reflection ellipsometry. Another PS film was used to create a PI/PS bilayer film by spin coating a solution of PI dissolved in heptane onto the PS film on mica. Heptane does not dissolve the underlying PS film. Solutions with a PI mass concentration of 1.2% were spin coated at a speed of 4000 rpm to obtain the PI film thicknesses h used in this study: $45 \text{ nm} < h < 56 \text{ nm}$. The PI/PS bilayer film was transferred onto a distilled water surface and captured across a 4-mm-diam hole in a stainless-steel sample holder, creating a freely standing PI/PS bilayer film. A portion of the PI/PS bilayer film was transferred onto a Si wafer for subsequent measurement of the PI/PS film thickness using reflection ellipsometry. To create a freely standing PS/PI/PS trilayer film, the water-transfer procedure was used to transfer a third, identical PS film from mica onto a freely standing PI/PS bilayer film which was then dried in filtered air. This resulted in a freely standing PS/PI/PS trilayer film in which the thicknesses of the PS capping layers were equal.

B. Experimental procedures for the measurement of lateral morphology

The lateral morphology which self-assembles in the freely standing PS/PI/PS trilayer films was characterized using reflected light microscopy. The films were placed in a custom-built hot stage on an Olympus BX-60 optical microscope. The optical microscopy images were collected using a Sony XC-70 three-color charge-coupled-device (CCD) camera interfaced to a Flashpoint frame grabber and analyzed using Image Pro Plus software.

To observe the formation of lateral morphology, the films were heated from room temperature to an elevated temperature $T < T_g^B = 97^\circ\text{C}$ for PS. Typically, the heating rate was fixed at a constant value ranging from 0.5 to $5^\circ\text{C}/\text{min}$, but some films were placed into the preheated optical microscope hot stage to achieve the fastest possible heating rate. Films were also subsequently heated to higher temperatures or cooled to lower temperatures to observe changes in the lateral morphology. The heating and cooling rates are specified below for each of the samples discussed.



FIG. 3. (Color online) Lateral morphology that has self-assembled in a freely standing PS/PI/PS trilayer film ($h=56 \text{ nm}$, $L=85 \text{ nm}$) upon heating to $T=95^\circ\text{C}$ at a rate of $2^\circ\text{C}/\text{min}$. The width of the image corresponds to $255 \mu\text{m}$.

A custom-built, single-wavelength ($\lambda=632.8 \text{ nm}$), self-nulling ellipsometer was used to measure the PS films and PI/PS bilayer films that had been transferred onto Si wafers. The film thickness and index of refraction were obtained from the measured ellipsometry angles assuming an isotropic, homogeneous film or bilayer film on an underlying substrate consisting of a 2-nm-thick SiO_x layer on Si. The index of refraction values used for SiO_x and Si for a wavelength of $\lambda=632.8 \text{ nm}$ were $n_{\text{SiO}_x}=1.460$ and $n_{\text{Si}}=3.886-0.02i$. This data fitting procedure has been shown to yield excellent fits to the ellipsometry data [18,19]. The absolute accuracy of the film thickness measurement is approximately 0.5 nm for the films used in the present study.

IV. RESULTS AND DISCUSSION

Following the room-temperature preparation of the freely standing PS/PI/PS trilayer films, the films were flat with only a small number of defects produced by the incorporation of dust particles and the use of a multiple-step water-transfer procedure which can produce cracks in the thin PS layers. As the flat trilayer films were heated from room temperature, the films were observed to wrinkle due to larger thermal expansion for the polymer trilayer films than for the stainless-steel sample holder and a lateral morphology consisting of a periodic banded structure was observed to form in the films. In Fig. 3 is shown an optical microscope image obtained at $T=95^\circ\text{C}$ for a freely standing PS/PI/PS trilayer film that was heated from room temperature at a rate of $2^\circ\text{C}/\text{min}$. The lateral morphology consists of a periodic, banded structure that contains regions in which the PI thickness is less than that in the original trilayer film (“pinched-off” regions) that are separated by regions in which the PI thickness is greater than that in the original trilayer film (PI “tubes”) (see Fig. 2).

For freely standing PS/PI/PS trilayer films that were heated quickly to an elevated temperature $T < T_g^B$, the bulk glass transition temperature for PS, undulations in the PI layer formed with a wavelength which decreased with increasing T . In Fig. 4 are shown the measured wavelengths of the lateral morphology as a function of temperature for PS/

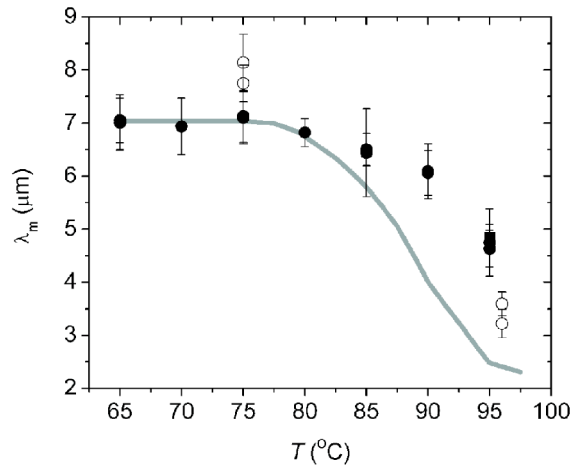


FIG. 4. Measured wavelength λ_m of the lateral morphology versus temperature T for a series of PS/PI/PS freely standing trilayer films which have PI thicknesses $45 \text{ nm} < h < 53 \text{ nm}$ and PS thicknesses $73 \text{ nm} < L < 79 \text{ nm}$. The solid symbols correspond to data collected for films heated quickly from room temperature to the temperature indicated on the plot. The open symbols correspond to data collected for films heated from room temperature at a rate of $4^\circ\text{C}/\text{min}$ to $T=96^\circ\text{C}$, held at $T=96^\circ\text{C}$ for 5 min, and then cooled at a rate of $4^\circ\text{C}/\text{min}$ to $T=75^\circ\text{C}$. The solid curve was obtained from an analysis of the data presented in Figs. 9 and 10, together with Eq. (11) (see text for details).

PI/PS trilayer films with $45 \text{ nm} < h < 53 \text{ nm}$ and $73 \text{ nm} < L < 79 \text{ nm}$ that were heated to different temperatures by placing the samples into the microscope hot stage that was preheated to the target temperature. There is essentially no change in the wavelength of the lateral morphology for temperatures $T < 75^\circ\text{C}$.

If a film was held at the elevated temperature for an extended time, the amplitude of the undulations in the PI layer was observed to grow with time, leading to the formation of distinct PI tubes separated by regions in which the separation between the two PS layers was very small. Once the lateral morphology began to form with a particular wavelength characteristic of a particular temperature, the wavelength did not change measurably upon further heating (for $T < T_g^B$ of PS), with the amplitude of the undulations in the PI layer increasing with time. In Fig. 5, optical microscope images are shown for two trilayer films (layer thicknesses $h = 50 \text{ nm}$ and $L = 60 \text{ nm}$) that have both been heated at a slow rate of $1^\circ\text{C}/\text{min}$ and differ only in the maximum temperature reached: 90°C for the film in Fig. 5(a), and 100°C for the film in Fig. 5(b). The domains are more distinct for the film heated to the higher temperature than for the film heated to the lower temperature. However, the wavelengths of the two morphologies agree to within 10%, which is the measured sample-to-sample variation in the wavelengths measured for different identical films heated to the same temperature.

A sequence of optical microscope images is shown in Fig. 6 for a freely standing PS/PI/PS film that was heated from room temperature at a constant heating rate of $1^\circ\text{C}/\text{min}$. With increasing temperature, the lateral morphology appears (images B and C) and then disappears (images E and F). In

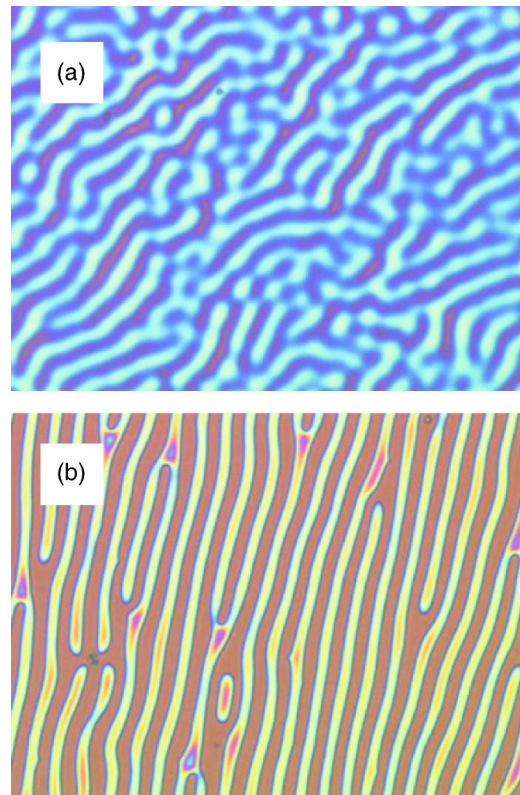


FIG. 5. (Color online) Optical microscope images for two freely standing PS/PI/PS trilayer films ($h=50 \text{ nm}$, $L=60 \text{ nm}$). Both films were heated from room temperature at a rate of $1^\circ\text{C}/\text{min}$. The image in part (a) was captured immediately after reaching $T=90^\circ\text{C}$, and the image in part (b) was captured immediately after reaching $T=100^\circ\text{C}$. The width of each image corresponds to $127 \mu\text{m}$.

image F, the film is remarkably uniform in color, indicating that the undulations in the film thickness that are most visible in image D have essentially been removed at the higher temperature. In images F, G, and H, corresponding to temperatures $T > T_g^B$, holes are observed to form and grow in the central PI layer [20]. The variation in intensity from top to bottom in image B is due to the presence of a long-wavelength wrinkle which forms in the polymer trilayer film as it is heated due to differential thermal expansion between the film and stainless-steel sample holder. A time sequence of optical microscope images, from which the images in Fig. 6 have been selected as a subset, is also available [21]. Below, we describe our measurements of the onset of the formation of lateral morphology formed by heating the films at a constant rate and the disappearance of the lateral morphology upon further heating, as well as the disappearance and reforming of the lateral morphology upon cooling. All of these results can be understood in terms of the time and temperature dependence of the viscoelastic properties of the PS capping layers.

A. Onset of lateral morphology upon heating

For films heated from room temperature at different constant heating rates, the lateral morphology was observed to

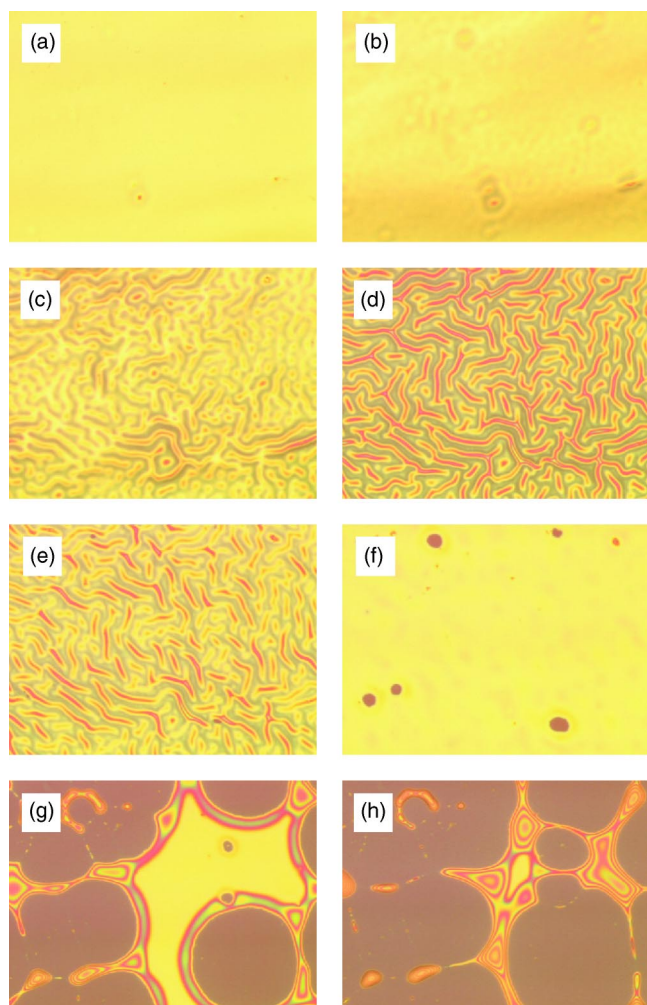


FIG. 6. (Color online) Optical microscopy images of a PS/PI/PS freely standing trilayer film ($h=56$ nm, $L=85$ nm) that was heated from 50 to 110°C at 1°C/min. The width of each image corresponds to 255 μ m. The letters correspond to specific temperatures: A, 66°C; B, 87°C; C, 90°C; D, 94°C; E, 97°C; F, 102°C; G, 109°C; H, 110°C.

form at a temperature that increased with increasing heating rate. To obtain a reliable measure of the onset temperature T_{onset} of the lateral morphology, we have calculated the average variance of the blue channel content of a series of optical microscope images collected at regular temperature increments during the heating of the films. For each pixel in the image, the average variance is computed as the sum of the squares of the difference between the intensity value for that pixel and those of its eight nearest-neighbor pixels, divided by the number of nearest-neighbor pixels [22]. For a film of uniform color, the average variance is zero. However, if there are short-range variations in the intensity of light with position in the image, the average variance is greater than zero. To select the best color channel for the calculation of the average variance, we plotted the 8-bit intensity values of each color channel measured using the CCD camera, together with the standard deviation of each intensity value, as a function of temperature for each sample. A representative plot of intensity versus temperature is shown for the blue

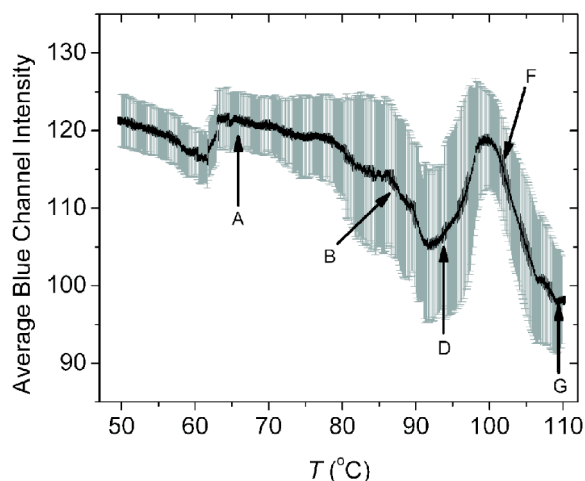


FIG. 7. Average blue channel intensity versus temperature for the optical microscopy images corresponding to the same trilayer film as in Fig. 6. The error bars indicated for each data point correspond to the standard deviation of the blue channel intensity in the optical image. The letters refer to the specific images shown in Fig. 6, indicating the formation of the lateral morphology (B), the disappearance of the morphology (F), and the formation of holes in the central PI layer (G).

channel in Fig. 7 for the same PS/PI/PS trilayer film as in Fig. 6. We chose the blue channel because the intensity values plus or minus the standard deviation of the intensity values did not reach the maximum (255) or minimum (0) intensity values over the entire temperature range for all of the samples.

For a series of freely standing PS/PI/PS trilayer films with $h=56$ nm and $L=85$ nm heated at different constant rates, we have computed the average variance per pixel as a function of temperature for optical microscope images collected at regular temperature increments. The average variance versus temperature is shown in Fig. 8 for the same PS/PI/PS film as in Fig. 6. Initially, the variance is small, since the images are of uniform color, corresponding to uniform film thickness. At higher temperatures, two peaks are observed in the average variance: the peak observed at $T \approx 95^\circ\text{C}$ corresponds to the formation and disappearance of the lateral morphology and the peak observed at $T \approx 109^\circ\text{C}$ corresponds to the formation and growth of holes in the central PI layer. Discontinuous jumps in the average variance, such as those observed for $T=93^\circ\text{C}$ and 107°C in Fig. 8, are due to the manual refocusing of the optical microscope during the experiment. For each film, T_{onset} was determined from the low-temperature peak in the average variance by fitting straight lines to the data for temperatures below and above T_{onset} (see inset to Fig. 8). The average values of the T_{onset} values obtained at each heating rate are plotted as a function of heating rate in Fig. 9. The error bars correspond to the standard deviation of the T_{onset} values measured for that heating rate. An increase in T_{onset} of about 10°C was observed as the heating rate was increased by a factor of 4. Additional measurements were performed for a heating rate of 5°C/min, but formation of the lateral morphology was obscured by hole formation in the central PI layer at this rapid heating rate.

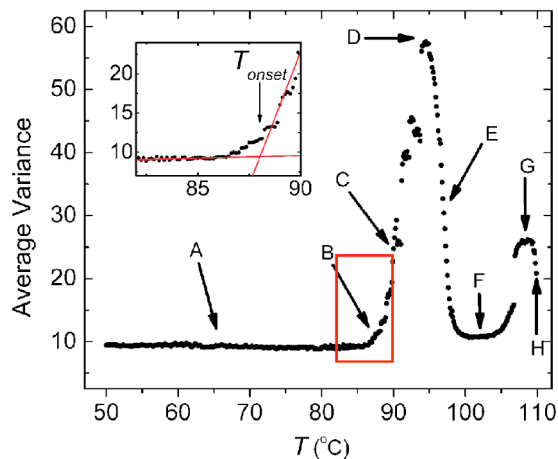


FIG. 8. Average variance per pixel of the blue channel intensity versus temperature calculated for the same trilayer film as in Fig. 6. The letters refer to the specific images shown in Fig. 6, indicating the formation of the lateral morphology (B), the disappearance of the morphology (F), and the formation of holes in the central PI layer (G). The inset shows the average variance versus time for the onset of the lateral morphology, together with straight line fits to the data above and below the onset temperature T_{onset} which is indicated by the vertical arrow.

The average variance technique for measuring the onset of the formation of lateral morphology is sensitive to short-range variations in the intensity in the images, since intensities in neighboring pixels are compared, and therefore it works very well for images such as those shown in Fig. 6 in which the wavelength of the morphology is much smaller than the lateral extent of the field of view. Changes to the intensity due to the formation of long-wavelength wrinkles in the film caused by differential thermal expansion between the polymer trilayer film and the stainless-steel sample holder can produce large variations in the average intensity, corresponding to the large standard deviation of the blue channel intensity for temperatures $80^\circ\text{C} < T < 90^\circ\text{C}$ in Fig. 7. Despite the presence of large standard deviations due to

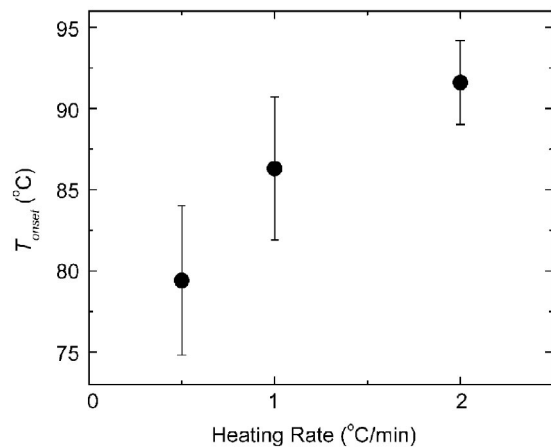


FIG. 9. Temperatures T_{onset} corresponding to the onset of lateral morphology as a function of heating rate. The error bars correspond to the standard deviation of the T_{onset} values measured for multiple samples for each heating rate.

long-wavelength variations in intensity, the contribution of such intensity variations to the average variance is small (see Fig. 8). Therefore, a sensitive measure of the onset of the lateral morphology from the average variance data can be obtained even if there are wrinkles in the film.

To understand the change in T_{onset} as a function of heating rate, as well as changes to the lateral morphology observed by changing the temperature T presented below, it is necessary to consider the effect of changing T on the stiffness of the PS capping layers. In the calculation presented above for the formation of lateral morphology in freely standing trilayer films, it was assumed that the central layer was fluid and the capping layers were solid at the temperature of the experiment. Although it is a good approximation that the central PI layer is a viscous fluid at the temperatures of interest (well above the glass transition temperature of $\sim -70^\circ\text{C}$ for PI), the Young's modulus Y of the PS capping layers can be a strong function of both the temperature and time scale of the experiment. In general, Y increases with decreasing time scale and temperature. Fujita and Ninomiya [23] have measured Young's modulus Y for polystyrene with molecular weight $M_w = 183 \times 10^3$ for different temperatures within the range $79^\circ\text{C} < T < 155^\circ\text{C}$ and for a range of times $60\text{ s} < t < 6000\text{ s}$. Using time-temperature superposition, they constructed a master curve of $Y(t)$ at a reference temperature of $T = 135^\circ\text{C}$. We have used their master curve of $Y(t)$ to generate curves of $\log_{10} Y(t)$ versus $\log_{10} t$ at different temperatures, as shown in Fig. 10(a) [24].

In the initial stages of lateral morphology formation, the morphology grows or decays with a characteristic time scale τ given by Eq. (12). In the temperature range corresponding to the present experiments, the dependence of τ on temperature is determined primarily by the temperature dependence of the Young's modulus Y of the PS capping layers and, to a lesser extent, the temperature dependence of the viscosity η of the PI layer. For PI at $T = 95^\circ\text{C}$ (which is 165°C above T_g), a 20°C decrease in temperature produces only a factor of approximately 1.9 increase in the viscosity, based on the Williams-Landel-Ferry (WLF) parameters for *cis*-1,4-PI [25]. By neglecting the small temperature dependence of η , rearranging Eq. (12) for Y , and taking the base-10 logarithm, we obtain

$$\log_{10} Y(T) = 2 \log_{10} \tau(T) - 2 \log_{10} C, \quad (13)$$

where C contains the terms that do not depend strongly on temperature. From Eq. (13), we can see that a plot of $\log_{10} Y$ versus $\log_{10} \tau$ has a slope of 2.

In Fig. 10(b) are shown the $Y(t)$ curves corresponding to the measured T_{onset} values shown in Fig. 9. Each data point corresponds to the intersection of a vertical line indicating the experimental time scale (taken to be the inverse of the heating rate) and the $Y(t)$ curve corresponding to the measured T_{onset} value (obtained by time-temperature superposition from the data in [23]). A line of slope 2, as predicted using Eq. (13), is also shown. Reasonable agreement between the measured data and the line of slope 2 is obtained, corresponding to a change in Young's modulus of about a

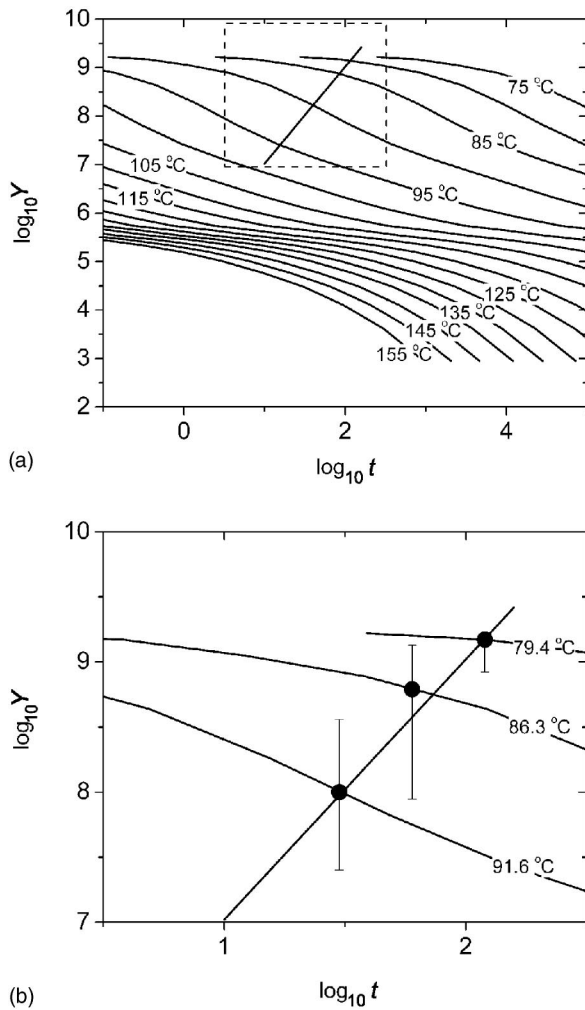


FIG. 10. (a) \log_{10} - \log_{10} plot of Young's modulus Y of PS in Pa as a function of time in seconds for different temperatures, derived from [22]. (b) An enlargement of the portion of the plot in part (a) indicated by the dashed lines. Each data point corresponds to the intersection of a vertical line indicating the experimental timescale (inverse of heating rate) and the $Y(t)$ curve corresponding to the measured value of T_{onset} . The straight line has slope 2.

factor of 10 for the time and temperature ranges of the measured onset of the lateral morphology.

B. Changes to the lateral morphology upon further heating and cooling

1. Experimental observations

After the lateral morphology has formed in the freely standing polymer trilayer films at an elevated temperature, we observe large, qualitative changes to the morphology upon further heating or cooling of the films. If the polymer trilayer film is heated to a temperature $T > T_g^B$ after the lateral morphology has formed, the lateral morphology disappears with time (see the images of Fig. 6). Specifically, the color of the film becomes uniform, indicating that the total film thickness is uniform in the plane of the film, just as it was following the preparation of the trilayer film. As the film

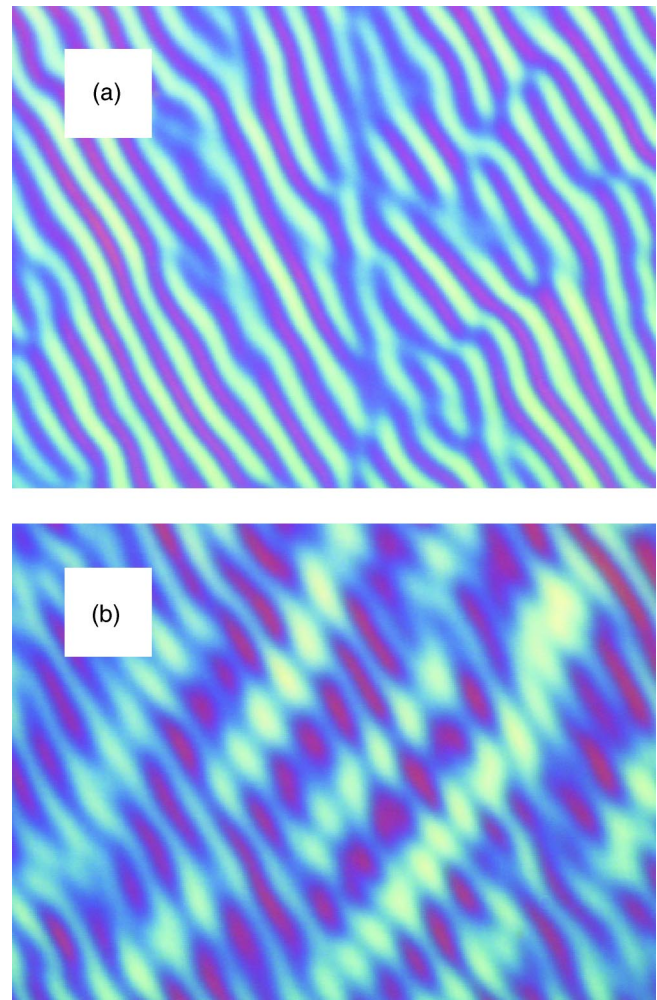


FIG. 11. (Color online) (a) Lateral morphology which has formed in a freely standing PS/PI/PS trilayer film ($h=49$ nm, $L=73$ nm) that has been heated to $T=96^\circ\text{C}$ at a rate of $4^\circ\text{C}/\text{min}$. The width of the image corresponds to $50\ \mu\text{m}$. (b) Lateral morphology observed for the same film as in part (a) after cooling the film to $T=75^\circ\text{C}$ at a rate of $4^\circ\text{C}/\text{min}$. The image was collected after 30 min at $T=75^\circ\text{C}$. The width of the image corresponds to $50\ \mu\text{m}$.

is further heated to temperatures $T > T_g^B$ for PS, holes form and grow in the central PI layer.

If instead the polymer trilayer film is cooled to a low temperature after the lateral morphology has begun to form at a high temperature $T < T_g^B$, we observe that the morphology characteristic of the high temperature disappears with time, while simultaneously a new morphology forms at right angles to the original morphology with a larger wavelength characteristic of the low temperature. An optical microscope image of the lateral morphology observed after heating a freely standing PS/PI/PS trilayer film to $T=96^\circ\text{C}$ at a rate of $4^\circ\text{C}/\text{min}$ is shown in Fig. 11(a). The film was then cooled at a rate of $4^\circ\text{C}/\text{min}$ to $T=75^\circ\text{C}$, and after 30 min at $T=75^\circ\text{C}$, the optical microscope image shown in Fig. 11(b) was obtained. In Fig. 11(b), both the original morphology characteristic of $T=96^\circ\text{C}$, with the smaller wavelength running diagonally from the top left to the bottom right, and the new morphology characteristic of $T=75^\circ\text{C}$, with the larger

wavelength running diagonally from the top right to the bottom left, can be seen.

2. Discussion

To understand the experimental observations presented above, we modify the linear stability analysis presented in the Introduction to account for the time and temperature dependence of Young's modulus Y of the PS capping layers. Specifically, we allow for three contributions to the free energy of the freely standing polymer trilayer system: (1) the creation of new surface, as determined by the PS surface tension, (2) the bending of the PS capping layers, and (3) the dispersion interaction acting across the total film thickness. In the presence of sinusoidal undulations $\zeta \cos qx$ in each outer film surface, symmetric about the midplane of the trilayer film (see Fig. 2), the average change in the free energy of the system is given by

$$\begin{aligned} \langle \Delta E \rangle &= \langle \Delta E_{\text{surf}} \rangle + \langle \Delta E_{\text{bend}} \rangle + \langle \Delta E_{\text{disp}} \rangle \\ &= \frac{2\gamma}{\lambda} \left\{ \int_0^\lambda \left[1 + \frac{1}{2} \left(\frac{dy}{dx} \right)^2 \right] dx - \lambda \right\} \\ &\quad + \frac{YL^3}{24\lambda(1-\sigma^2)} \left[\int_0^\lambda \left(\frac{d^2y}{dx^2} \right)^2 dx \right] \\ &\quad - \frac{A}{12\pi\lambda} \left[\int_0^\lambda \left(\frac{1}{(h+2L)^2} - \frac{1}{(h_0+2L)^2} \right) dx \right], \end{aligned} \quad (14)$$

where γ is the surface tension of the air/PS interface, Y and σ are the Young's modulus and Poisson's ratio for the PS layers, A is the Hamaker coefficient associated with the PS/air interface, h_0 is the unperturbed PI film thickness, $h=h_0+2\zeta \cos qx$ is the perturbed PI film thickness, $y=\zeta \cos qx$ is the undulation of one surface, and $\langle \dots \rangle$ refers to an average over one wavelength λ of the undulation.

At temperatures $T < T_g^B$ for the PS capping layers, the important contributions to Eq. (14) are the bending energy of the capping layers (since Y is relatively large in the glassy state) and the dispersion force [9]. At these temperatures, the viscosity of PS is very large and its elastic modulus is relatively high, such that the PS film cannot respond to the surface tension and this contribution is neglected in Eq. (14). This low-temperature case corresponds to the situation considered in the Introduction for freely standing trilayer films with solid capping layers and, in the limit of small-amplitude undulations ($\zeta \ll h_0$), Eq. (14) can be written as

$$\langle \Delta E_L \rangle = \left[\frac{YL^3}{24(1-\sigma^2)} (q^L)^4 - \frac{A}{2\pi(h_0+2L)^4} \right] \zeta^2, \quad (15)$$

corresponding to a critical wave vector $q_c^L = 2\pi/\lambda_c^L$ for which $\langle \Delta E_L \rangle = 0$ given by [see also Eq. (6)]

$$q_c^L = \frac{2\pi}{\lambda_c^L} = \sqrt[4]{\frac{12A(1-\sigma^2)}{\pi Y L^3 (h_0+2L)^4}}. \quad (16)$$

At temperatures $T > T_g^B$ for the PS capping layers, Y of the capping layers is relatively small and the PS films have a

TABLE I. Typical parameter values for PS/PI/PS trilayer films.

Parameter	Symbol	Value
Hamaker coefficient ^a	A	10^{-19} J
PS surface tension at $T=105^\circ\text{C}$	$\gamma(T=105^\circ\text{C})$	35 mN/m
PI thickness	h	50 nm
PS thickness	L	50 nm
PS Young's modulus ^b	Y	1.8×10^9 Pa
PS Poisson's ratio	σ	0.3
Ratio of PI viscosity at $T=75^\circ\text{C}$ to that at $T=105^\circ\text{C}$ ^c	$\eta(T=75^\circ\text{C})/\eta(T=105^\circ\text{C})$	2.4

^aTypical value of the Hamaker coefficient for the vacuum/PS/vacuum interface [26].

^bYoung's modulus at $T=75^\circ\text{C}$ and times $t < 10^3$ s [23].

^cCalculated using WLF parameters for PI [25].

sufficiently small viscosity that they can flow in response to the surface tension, such that the important contributions to the change in the free energy are the surface tension and the dispersion force terms in Eq. (14). This high-temperature case corresponds to the situation considered in the Introduction for freely standing single-layer fluid films, and in the limit of small-amplitude undulations ($\zeta \ll h_0$), Eq. (14) can be written as

$$\langle \Delta E_H \rangle = \left[\frac{(q^H)^2 \gamma}{2} - \frac{A}{2\pi(h_0+2L)^4} \right] \zeta^2, \quad (17)$$

corresponding to a critical wave vector $q_c^H = 2\pi/\lambda_c^H$ for which $\langle \Delta E_H \rangle = 0$, given by

$$q_c^H = \frac{2\pi}{\lambda_c^H} = \sqrt{\frac{A}{\pi\gamma(h_0+2L)^4}}. \quad (18)$$

If we substitute typical values for the parameters as listed in Table I into Eqs. (16) and (18), we see that in the low-temperature case, the value of the critical wave vector $q_c^L \approx 2.4 \times 10^5 \text{ m}^{-1}$ is larger than in the high-temperature case by a factor of approximately 5, and so the critical wavelength $\lambda_c^L \approx 0.2\lambda_c^H$. As the lateral morphology forms in the film at a temperature well below T_g^B for PS, it does so with the wavelength λ_m^L that grows most quickly, where $\lambda_m^L = \sqrt[4]{3} \lambda_c^L$ [9].

We can now use the above analysis to try to understand the changes in the lateral morphology observed experimentally, as detailed at the beginning of this section. The decrease in Y with increasing temperature (see Fig. 10) substantially reduces the contribution of the bending energy to the free energy at high temperatures. Concurrently, at high temperatures, the PS is more fluid like and can respond to the surface tension contribution in the free energy which acts to reduce the surface area of the film. Since the critical wavelength at high temperature, λ_c^H , is larger than the wavelength of the morphology, λ_m^L , which formed at a lower temperature, the morphology becomes unstable and the undulations in the film surfaces decay with time. This is in agreement with

experimental observations, in which the morphology is removed from the films at temperatures comparable to T_g^B (see Fig. 6).

The change in the lateral morphology observed upon cooling of the film from a relatively high temperature can also be understood on the basis of the time and temperature dependence of Y . As the temperature is decreased from 95 to 75 °C, Y will increase by a factor of 63, as determined by the intersection of the line of slope 2 with the $Y(t)$ curves for the two temperatures in Fig. 10(a). This means that the critical wavelength λ_c^L will increase by a factor of $\sqrt[4]{63} \approx 2.8$, such that it becomes larger than the wavelength λ_m^L of the existing undulation. As a result, the morphology which formed at high temperature becomes unstable and the amplitude of the undulation decays with time. At the same time, a lateral morphology with a larger wavelength characteristic of the lower temperature forms and its amplitude grows with time. This can be understood by realizing that excess surface area is required to allow lateral morphology to form in the films. The morphology can form upon initial heating of the films from room temperature because of the increase in the surface area of the film due to differential thermal expansion between the polymer film and the stainless-steel sample holder. Upon subsequent cooling to temperatures for which the morphology is observed to reform, there is a small reduction in the area of the films due to thermal contraction, but there is still more surface area for the film compared with that at room temperature. To create enough excess surface area for the morphology characteristic of the lower temperature to form, it is necessary for some of the initial, high-temperature morphology to decay. So the low-temperature morphology grows as the high-temperature morphology decays.

It is interesting to note that the low-temperature morphology forms essentially at right angles to the original, high-temperature morphology. This can be understood in terms of the amount by which the PI must be moved to achieve the new morphology. To form the larger wavelength morphology parallel to and in the presence of the original high-temperature morphology requires movement of entire PI domains to larger separation, producing large curvature of the PS capping layers. It is much more energetically favorable—i.e., involves less movement of PI and less bending of the PS capping layers—to form the larger-wavelength morphology at right angles to the original high-temperature morphology. For the film shown in Fig. 11, the angle between the low- and high-temperature morphologies was found to vary between 70° and 90° at different lateral positions in the film. The deviation from perpendicularity between the two morphologies is likely due to the presence of small, in-plane stresses obtained by thermally cycling the film which can cause the low-temperature morphology to form along a preferred direction in the plane of the film.

As shown in Fig. 4, the wavelength of the lateral morphology decreases with increasing temperature. This occurs

because of the decrease of Young's modulus of the PS capping layers with increasing temperature. Also included in Fig. 4 are data points (open symbols) obtained for two PS/PI/PS trilayer films that were heated at a rate of 4 °C/min to $T=96$ °C, held at $T=96$ °C for 5 min and then cooled at a rate of 4 °C/min to $T=75$ °C. The wavelengths measured for the reformed morphology at $T=75$ °C are the same to within the uncertainty of the measurement as the wavelengths measured for the morphology obtained by heating from room temperature to $T=75$ °C (solid circles). In addition, a solid curve is shown in Fig. 4 which was calculated from Eq. (11) using temperature-dependent Y values for 75 °C $< T < 95$ °C obtained from the intersection of the line of slope 2 and the $Y(t)$ curves shown in Fig. 10. To compare the measured and calculated wavelength values, the value of the calculated wavelength for $T < 85$ °C was adjusted to be equal to the measured values in this temperature range. The calculated temperature dependence of the wavelength values agrees remarkably well with the measured temperature dependence and this provides supporting evidence that the analysis of the onset temperature data presented above is valid. At the higher temperatures, the calculated wavelength values fall slightly below the measured values. Perhaps refinements to the calculation—e.g., nonlinear effects [27] or a complete description of the viscoelastic properties of PS—could account for these small differences.

V. SUMMARY AND CONCLUSIONS

We have used reflected light microscopy to study the lateral morphology which self-assembles at elevated temperatures in freely standing PS/PI/PS trilayer films. A detailed analysis is presented for the dependence on heating rate of the onset temperature T_{onset} for the formation of morphology. By changing the temperature of the trilayer films—i.e., further heating or cooling of the films—we have produced large changes in the morphology. In particular, further heating to temperatures above the glass transition temperature of PS causes the morphology to disappear with time. Alternatively, cooling of the films causes the original high-temperature morphology to disappear and simultaneously reform at right angles to the original morphology with a larger wavelength characteristic of the lower temperature. The dependence of T_{onset} on heating rate and changes in morphology with increasing or decreasing temperature can be understood in terms of the time and temperature dependence of Young's modulus of the PS capping layers.

ACKNOWLEDGMENTS

We thank Dr. B.G. Nickel for stimulating discussions. Financial support from NSERC of Canada, the Canada Foundation for Innovation, and the Ontario Innovation Trust is gratefully acknowledged.

- [1] J. N. Israelachvili, *Intermolecular & Surface Forces*, 2nd ed. (Academic, San Diego, 1991).
- [2] G. Reiter, *Phys. Rev. Lett.* **68**, 75 (1992).
- [3] F. Brochard-Wyart and J. Daillant, *Can. J. Phys.* **68**, 1084 (1990).
- [4] G. Debrégeas, P. Martin, and F. Brochard-Wyart, *Phys. Rev. Lett.* **75**, 3886 (1995).
- [5] G. Debrégeas, P.-G. de Gennes, and F. Brochard-Wyart, *Science* **279**, 1704 (1998).
- [6] K. Dalnoki-Veress, B. G. Nickel, C. Roth, and J. R. Dutcher, *Phys. Rev. E* **59**, 2153 (1999).
- [7] J. D. Gunton, M. San Miguel, and P. S. Sahni, in *Phase Transitions and Critical Phenomena*, edited by C. Domb and J. L. Lebowitz (Academic Press, London, 1983).
- [8] A. Vrij and J. Th.G. Overbeek, *J. Am. Chem. Soc.* **90**, 3074 (1968).
- [9] K. Dalnoki-Veress, B. G. Nickel, and J. R. Dutcher, *Phys. Rev. Lett.* **82**, 1486 (1999).
- [10] M. O. David, G. Reiter, T. Sitthai, and J. Schultz, *Langmuir* **14**, 5667 (1998).
- [11] G. Reiter, A. Sharma, A. Casoli, M. O. David, R. Khanna, and P. Auroy, *Europhys. Lett.* **46**, 512 (1999).
- [12] E. Schäffer, T. Thurn-Albrecht, T. P. Russell, and U. Steiner, *Nature (London)* **403**, 874 (2000).
- [13] E. Schäffer, S. Harkema, R. Blossey, and U. Steiner, *Europhys. Lett.* **60**, 255 (2002).
- [14] S. Y. Chou, L. Zhuang, and L. Guo, *Appl. Phys. Lett.* **75**, 1004 (1999).
- [15] S. Y. Chou and L. Zhuang, *J. Vac. Sci. Technol. B* **17**, 3197 (1999).
- [16] J. M. Thomas, C. A. Murray, and J. R. Dutcher (unpublished).
- [17] L. D. Landau and E. M. Lifshitz, *Theory of Elasticity*, 3rd ed. (Pergamon, Oxford, 1986), pp. 38–40.
- [18] J. A. Forrest, K. Dalnoki-Veress, and J. R. Dutcher, *Phys. Rev. E* **56**, 5705 (1997).
- [19] K. Dalnoki-Veress, J. A. Forrest, C. A. Murray, C. Gigault, and J. R. Dutcher, *Phys. Rev. E* **63**, 031801 (2001).
- [20] C. A. Murray, J. M. Thomas, and J. R. Dutcher (unpublished).
- [21] See EPAPS Document No. E-PLIEEE8-69-079406 for a time sequence of optical microscopy images of a PS/PI/PS freely standing trilayer film ($h=56$ nm, $L=85$ nm) that was heated from 50 to 110°C at 1°C/min. The width of each image corresponds to 255 μm. A direct link to this document may be found in the online article's HTML reference section. The document may also be reached via the EPAPS homepage (<http://www.aip.org/pubservs/epaps.html>) or from <ftp.aip.org> in the directory /epaps/. See the EPAPS homepage for more information.
- [22] J. C. Russ, *The Image Processing Handbook*, 3rd ed. (CRC Press, Boca Raton, 1999).
- [23] H. Fujita and K. Ninomiya, *J. Polym. Sci.* **24**, 233 (1957).
- [24] We note that the master curve of $Y(t)$ obtained by Fujita and Ninomiya [22] was determined for PS with molecular weight $M_w=183\times 10^3$, and we have used PS with molecular weight $M_w=717\times 10^3$ in the present study. To obtain the master curve of $Y(t)$ for the present case, it is necessary to modify the $Y(t)$ curve to include the scaling of the terminal time τ^* with molecular weight M_w , $\tau^* \sim M_w^{3.4}$, which extends the plateau region to longer times. However, for the times and temperatures that are relevant to the present study [see Fig. 10(b)], the extension of the plateau region to longer times for the larger value of M_w is not important, and we have used the master curve of Fujita and Ninomiya to generate the $Y(t)$ curves shown in Fig. 10.
- [25] Williams-Landel-Ferry parameter values of $T_0=250$ K, $C_1=6.1$, and $C_2=70.9$ K for *cis*-1,4-PI with a molecular weight of 97×10^3 g/mol, from *Physical Properties of Polymers Handbook*, edited by J. E. Mark (Springer-Verlag, New York, 1996).
- [26] J. Visser, *Adv. Colloid Interface Sci.* **3**, 331 (1972).
- [27] T. Erneux and S. H. Davis, *Phys. Fluids A* **5**, 1117 (1993).